Published OnlineFirst October 16, 2012; DOI: 10.1158/0008-5472.CAN-12-2071

Therapeutics, Targets, and Chemical Biology

Cancer Research

Superior Penetration and Retention Behavior of 50 nm Gold Nanoparticles in Tumors

Shuaidong Huo[1,2], Huili Ma[2], Keyang Huang[2], Juan Liu[2], Tuo Wei[2], Shubin Jin[2], Jinchao Zhang[3], Shengtai He[1], and Xing-Jie Liang[2]

Abstract

Nanoparticles offer potential as drug delivery systems for chemotherapeutics based on certain advantages of molecular drugs. In this study, we report that particle size exerts great influence on the penetration and retention behavior of nanoparticles entering tumors. On comparing gold-coated Au@tiopronin nanoparticles that were prepared with identical coating and surface properties, we found that 50 nanoparticles were more effective in all *in vitro*, *ex vivo*, and *in vivo* assays conducted using MCF-7 breast cells as a model system. Beyond superior penetration in cultured cell monolayers, 50 nm Au@tiopronin nanoparticles also penetrated more deeply into tumor spheroids *ex vivo* and accumulated more effectively in tumor xenografts *in vivo* after a single intravenous dose. In contrast, larger gold-coated nanoparticles were primarily localized in the periphery of the tumor spheroid and around blood vessels, hindering deep penetration into tumors. We found multicellular spheroids to offer a simple *ex vivo* tumor model to simulate tumor tissue for screening the nanoparticle penetration behavior. Taken together, our findings define an optimal smaller size for nanoparticles that maximizes their effective accumulation in tumor tissue. *Cancer Res; 73(1); 319–30. ©2012 AACR.*

Introduction

The ultimate objective of chemotherapy was to specifically kill the cancer cells without any adverse effects. In the past few decades, nanoparticle-based drug delivery system has shown unique advantages over small molecules. Some commercially available nanomedicines are widely used in the clinic for cancer therapy, including liposomes such as Doxil (liposome loaded with doxorubicin) and nanoparticles such as Abraxane (albumin nanoparticle loaded with paclitaxel). Because of prolonged circulation time and the altered biodistribution of the chemotherapeutic agent as well as the enhanced drug solubility of these commercial nanoparticles, the side effect of the drug was significantly reduced, whereas the efficacy of the drug was, to some extent, restricted because of the limited nanoparticle penetration into the tumor tissues (1). Generally, the anticancer drugs must penetrate into tumor tissues efficiently and reach to all of the cancer cells in a sufficient concentration to exert effective therapeutic efficacy (2).

In solid tumors, the microenvironment was complicated, with poorly organized vascular architecture, hypoxia, and increased interstitial fluid pressure as well as the presence of the extracellular matrix (ECM; refs. 3–5). These characteristics of the tumor microenvironment will significantly limit the delivery of drugs to the cells distant from the blood vessels, and then the efficiency of drug will be subsequently compromised. Compared with molecular drugs, the penetration behavior of the nanoparticles *in vitro* also depends on their properties, including size (6), shape (7), surface charge (8), the stage of the cell cycle (9), and so on.

Different from cells in monolayer culture, cells in solid tumor are exposed to the microenvironment described earlier and to a gradient of drug concentrations due to their distance from the blood vessels. In theory, direct *in vivo* evaluation of the penetration behavior of the nanoparticles is the most ideal way owing to the pharmacokinetics of nanoparticles that will significantly affect their accumulation in tumor tissue (10). Hence, the *ex vivo* model system is more simple and practicable to evaluate drug penetration, and the multicellular spheroid model is one of the most often used methods. Multicellular spheroids are spherical aggregates of tumor cells that reflect many properties of the solid tumor microenvironment(2, 11–14). Recently, it has been reported that the 3-dimensional (3D) culture system may better reflect some of the *in vivo* aspects and can be used to further improve the understanding of the molecular mechanism of action of Herceptin (14). In the present study, the breast cancer cell line MCF-7 tumor spheroid was developed, characterized, and used to qualitatively and

Authors' Affiliations: [1]School of Materials Science and Engineering, Tianjin Polytechnic University, Tianjin; [2]CAS Key Laboratory for Biological Effects of Nanomaterials and Nanosafety, National Center for Nanoscience and Technology, Beijing; and [3]College of Chemistry and Environmental Science, Chemical Biology Key Laboratory of Hebei Province, Hebei University, Baoding, China

Note: Supplementary data for this article are available at Cancer Research Online (http://cancerres.aacrjournals.org/).

S. Huo and H. Ma contributed equally to this work.

Corresponding Authors: Shengtai He, School of Materials Science and Engineering, Tianjin Polytechnic University, Tianjin 300387, China. Phone: 86-22-83955360; E-mail: shengtai.he@gmail.com; and Xing-Jie Liang, National Center for Nanoscience and Technology, No. 11, First North Road, Zhongguancun, Haidian district, Beijing 100190, China. Phone: 86-10-82545569; Fax: 86-10-62656765; E-mail: liangxj@nanoctr.cn

doi: 10.1158/0008-5472.CAN-12-2071

Published OnlineFirst October 16, 2012; DOI: 10.1158/0008-5472.CAN-12-2071

quantitatively evaluate the penetration and retention behavior of nanoparticles.

The enhanced permeation and retention (EPR) effect contributed to the passive tumor-targeting of nanoparticles with the size smaller than 100 nm (10, 15). The sizes of Doxil and Abraxane mentioned above are approximately 100 and 130 nm, respectively, and it was found that these nanoparticles were predominantly located near the blood vessels (1). Hence, size of the nanoparticles plays a critical role in their penetration and retention within the tumor tissue (6, 10, 16, 17). The 50 nm nanoparticles, including gold, silica, and polystyrene nanoparticles, were those that were taken up the most by monolayer cells (18–22). However, the systematic evaluation of the penetration of nanoparticles into the monolayer cells, tumor spheroid, and tumor tissue *in vivo* was not well understood until now. Gold nanoparticles have shown unique advantages in nanoparticle-based drug delivery systems due to significant improvements in the synthesis of gold nanoparticles with their ease of fabrication, controllable size and shape, good biocompatibility, tunable surface functionalities, and so on (7, 8, 10, 19, 20). Therefore, gold nanoparticles with different sizes and similar surface properties were selected in this study. Here, we hypothesized that smaller nanoparticles have advantages over the larger ones in terms of penetration behavior not only in tumor monolayer cells but also the tumor tissue *in vivo* (Scheme 1).

To prove our hypothesis, we systematically evaluated whether smaller gold nanoparticles were beneficial for penetration into cancer cells in monolayer cells *in vitro*, tumor spheroids *ex vivo*, and tumor tissues *in vivo*. First, we prepared the gold nanoparticles that measured 50 and 100 nm with identical surface coatings of tiopronin (Au@tiopronin NP). Tiopronin, a thiol drug with good biocompatibility, is used to control the rate of cysteine precipitation and excretion in cystinuria (23). In addition, tiopronin is used as a stabilizing agent for metal nanoparticles because its thiol groups can bind on the surface of nanoparticles to prevent coagulation (24). More importantly, the carboxyl groups of tiopronin can be modified with molecules, peptides, or drugs. In our previous work, Au@tiopronin NPs that were functionalized with the targeted and therapeutic peptides showed enhanced efficacy of cancer therapy (25). Then, the MCF-7 tumor spheroid as an *ex vivo* model was developed and characterized to study, in particular, the penetration and retention behavior of the gold nanoparticles. Furthermore, evaluation of the pharmacokinetics and biodistribution of the nanoparticles *in vivo* were carried out in the tumor-bearing mice.

Materials and Methods

Chemicals

Gold chloride trihydrate (≥99.9%, $HAuCl_4 \cdot 3H_2O$) and *N*-(2-mercaptopropionyl) glycine (tiopronin, $C_5H_9NO_3S$) were purchased from Sigma-Aldrich. L(+)-Ascorbic acid (99.0%) was supplied by Acros. Sodium citrate (≥99.5%, $C_6H_5Na_3O_7 \cdot 2H_2O$) was obtained from Solarbio. Nitric acid and hydrogen peroxide of metal–oxide–semiconductor (MOS) grade were bought from the Beijing Chemical Reagents Institute (Beijing, China). Stock standard solution of Au (1,000 μg/mL) was obtained from the National Analysis Center for Iron and Steel (Beijing, China). All glassware used for the preparation and storage of gold nanoparticles were cleaned with aqua regia (HCl: HNO_3 = 3:1, v/v). All chemicals were used without further purification, and Milli-Q water was used throughout this study.

Synthesis of 15 nm Au@citrate seed nanoparticles

Using the standard citrate reduction method, 15-nm Au@citrate NPs were prepared as reported previously (26). Briefly, 0.5 mL of $HAuCl_4 \cdot 3H_2O$ solution (1%, w/v) in 50 mL of Milli-Q water was heated to boiling and then 1.5 mL of sodium citrate solution (1%, w/v) was added to the boiling solution quickly

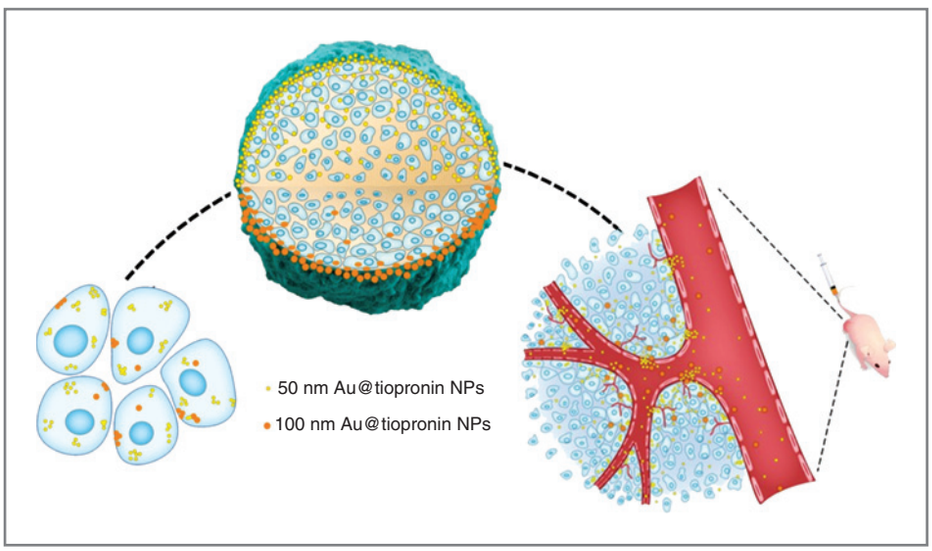

Scheme 1. Schematic illustration of the localization and penetration behavior of 50 and 100 nm Au@tiopronin nanoparticles in monolayer cancer cells *in vitro*, multicellular tumor spheroid *ex vivo*, and xenograft tumor model *in vivo*.

Published OnlineFirst October 16, 2012; DOI: 10.1158/0008-5472.CAN-12-2071

with vigorous stirring. After the color change was completed in 5 minutes, the mixture solution was kept boiling for another 15 to 30 minutes and, then, was allowed to cool down to room temperature with stirring. Finally, the15 nm Au@citrate NPs were obtained, and the nanoparticles were kept as the seed solution to synthesize larger gold nanoparticles measuring 50 and 100 nm.

Synthesis of 50 and 100 nm Au@citrate nanoparticles

Both 50 and 100 nm Au@citrate NPs were synthesized using the seed growth method (27). Generally, 2.25 mL of 15 nm Au@citrate nanoparticle seed solution was mixed with 2.44 mL of $HAuCl_4 \cdot 3H_2O$ solution (10 mmol/L) and the mixture was diluted to 150 mL with Milli-Q water. Then, 100 mL of ascorbic acid solution (0.4 mmol/L) was added to the above stirring solution at a rate of 10 mL/min with a peristaltic pump. Finally, the 50 nm Au@citrate NPs in purple red were obtained. For the preparation of 100 nm Au@citrate NPs, the method was the same as that of 50 nm Au@citrate NPs, with the exception that the volume of seed solution and $HAuCl_4 \cdot 3H_2O$ solution (10 mmol/L) were 0.24 and 2.49 mL, respectively.

Synthesis of 50 and 100 nm Au@tiopronin nanoparticles

In our study, a surface molecule exchange reaction was adopted to obtain 50 and 100 nm Au@tiopronin NPs using the corresponding Au@citrate NPs. Briefly, the reaction was carried out with stirring at 40°C for more than 48 hours by mixing a certain volume of as prepared Au@citrate NPs with an aqueous solution containing excess of tiopronin. When the reaction was completed, both Au@citrate and Au@tiopronin NPs were centrifuged 3 times at 10,000 rpm for 30 minutes to remove any residual salt, unbound tiopronin, and citrate.

To characterize all the gold nanoparticles mentioned earlier, including 15 nm Au@citrate NPs, 50 and 100 nm Au@citrate NPs, and 50 and 100 nm Au@tiopronin NPs, some instruments including the Tecnai G^2 20 S-TWIN Transmission Electron Microscope (TEM; Philips) with 200 kV acceleration voltage, Nano ZS Zetasizer (Malvern), X-ray photoelectron spectrometer (XPS; ESCALAB250Xi X-ray photoelectron spectrometer; Thermo Fisher Scientific), Lambda 950 UV/vis/NIR spectrophotometer (Perkin-Elmer), and X-ray diffractometer (XRD; X′Pert PRO MPD X-ray diffractometer; PANalytical B.V.) were used in this work.

Uptake of gold nanoparticles by monolayer MCF-7 cells

The human breast cancer cell line MCF-7 was maintained in Dulbecco's Modified Eagle's Medium with 10% FBS in a humidified atmosphere containing 5% CO_2 at 37°C. MCF-7 cells were cultured in 6-well plates at approximately 60% confluence. Thereafter, the medium was removed and 1 mL of fresh medium containing 50 or 100 nm Au@tiopronin NPs at a dose of 1 nmol/L was added to the wells. After the 24-hour incubation, cells were washed gently with 150 mmol/L PBS (pH 7.4), digested with 0.25% trypsin-EDTA, centrifuged at 1,000 rpm for 3 minutes, then collected and counted by Vi-CELL (Beckman Coulter).

MCF-7 multicelluar spheroid culture

The MCF-7 spheroid was produced by using the liquid overlay method as previously described (28). Briefly, cells were detached from the monolayer and single-cell suspension and were transferred into a flat-bottomed 96-well plate precoated with 1% agarose (w/v) at a dose of 200 μL per well containing 600 cells. Afterwards, the cells were incubated for approximately 7 days in the same condition as the monolayer cells described previously. In addition, the culture medium was partially (100 μL) replaced by fresh medium every other day.

Penetration behavior of gold nanoparticles into spheroids

For the 7-day-old spheroid at the seeding concentration of 600 cells per well, 100 μL medium was replaced by medium containing 50 or 100 nm Au@tiopronin NPs at a concentration of 2 nmol/L; therefore, the final treated concentration is 1 nmol/L. After the 24-hour incubation, the spheroids were taken out using a pipette, and gently washed with PBS for the following analysis. The distribution of gold nanoparticles in the spheroid was qualitatively observed using microscopy under bright and dark fields. The ultralocalization of gold nanoparticles in the outer and inner cells of the spheroid was evaluated by Bio-TEM (JEM-1400; JEOL). In addition, the gold content in every spheroid was quantified by inductively coupled plasma mass spectrometry (ICP-MS; ELAN DRC-e inductively coupled plasma mass spectrometer; Perkin-Elmer).

Pharmacokinetics and biodistribution of gold nanoparticles in tumor-bearing mice

Female balb/c nude mice (18–20 g) were purchased from Beijing Vital River Laboratories. All care and handling of animals was carried out with the approval of the Animal Ethics Committee of the Medical School, Peking University (Beijing, China). To establish the tumor-bearing mice, the mice were subcutaneously inoculated with 4×10^6 cells into the right flank of the mice. When the average volume of the tumor reached approximately 100 mm^3, the mice were randomly divided into groups for the study of pharmacokinetics and distribution of Au@tiopronin NPs.

For pharmacokinetics study, the tumor-bearing mice were intravenously injected with 50 and 100 nm Au@tiopronin NPs at a dose of 5 mg Au/kg. About 30 to 100 μL blood was taken for sampling from the tail vein with a quantitative capillary at 10 minutes and 1, 3, 8, and 24 hours after administration. In addition, the nanoparticles were injected in the lower part of one tail vein, and the blood sample was taken from the other end of the tail vein, thereby protecting the sample from contamination. The blood volume was calculated as 0.0778 mL/g body weight, and the blood samples were used to measure gold content using ICP-MS. For the tissue distribution evaluation, tissues including tumor, heart, liver, spleen, lung, and kidney were removed at 24 hours after the injection, and a part of the collected tissues were used for ICP-MS measurement, Bio-TEM observation, and histologic evaluation, respectively.

Published OnlineFirst October 16, 2012; DOI: 10.1158/0008-5472.CAN-12-2071

Result and Discussion

Characterization of 50 and 100 nm Au@citrate NPs

To obtain 50 and 100 nm Au@citrate NPs, 15 nm Au@citrate NPs were first prepared as seeds. As shown in Supplementary Fig. S1A and S1B, the prepared 15 nm Au@citrate NPs showed uniform spherical morphology measuring 14.8 ± 0.6 nm and possessing ζ potential of −23.8 mV. In addition, the 15 nm Au@citrate NPs were red in color, with maximum adsorption at 519 nm as shown in the visible absorption spectrum (Supplementary Fig. S1C). The results in Fig. 1 revealed that the sizes of the Au@citrate NPs were 49.8 ± 6.6 and 101.1 ± 13.8 nm and

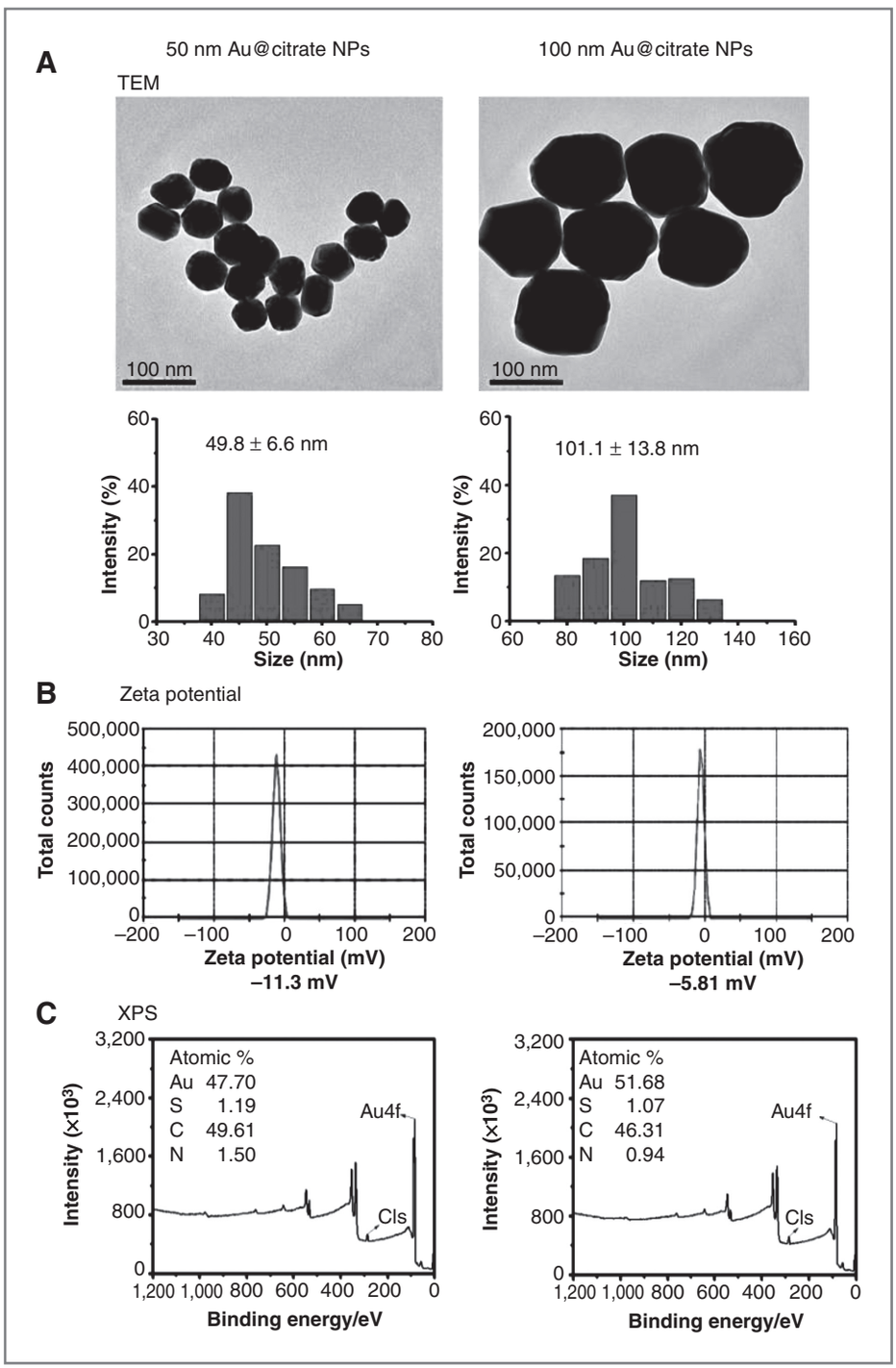

Figure 1. Characterization of 50 and 100 nm Au@citrate nanoparticles. A, TEM images and the corresponding size histograms of as-synthesized 50 and 100 nm gold nanoparticles coated with citrate. B, zeta potential of the above nanoparticles. C, XPS graph of the Au@citrate nanoparticles for 50 and 100 nm, which showed the atomic percentage of C, N, S, and Au in the nanoparticles.

Published OnlineFirst October 16, 2012; DOI: 10.1158/0008-5472.CAN-12-2071

the ζ-potential of the 50 nm and 100 nm Au@citrate NPs were −11.3 and −5.8 mV, respectively.

Characterization of 50 and 100 nm Au@tiopronin NPs

Both 50 and 100 nm Au@tiopronin NPs were successfully obtained in this study. Because of the higher binding affinity of thiol groups to gold in comparison with the electrostatic interaction between gold nanoparticles and citrate, 50 and 100 nm Au@tiopronin NPs were prepared by the surface exchange of tiopronin with corresponding Au@citrate NPs. In Fig. 2A, the 50 and 100 nm Au@tiopronin NPs measured 50.7 ± 6.7 and 102.6 ± 11.2 nm respectively, indicating that the size of the Au@tiopronin NPs had barely changed after the surface exchange of tiopronin with the corresponding Au@citrate NPs. Compared with the corresponding Au@citrate NPs in Fig. 2B, the ζ-potentials of 50 and 100 nm Au@tiopronin NPs decreased

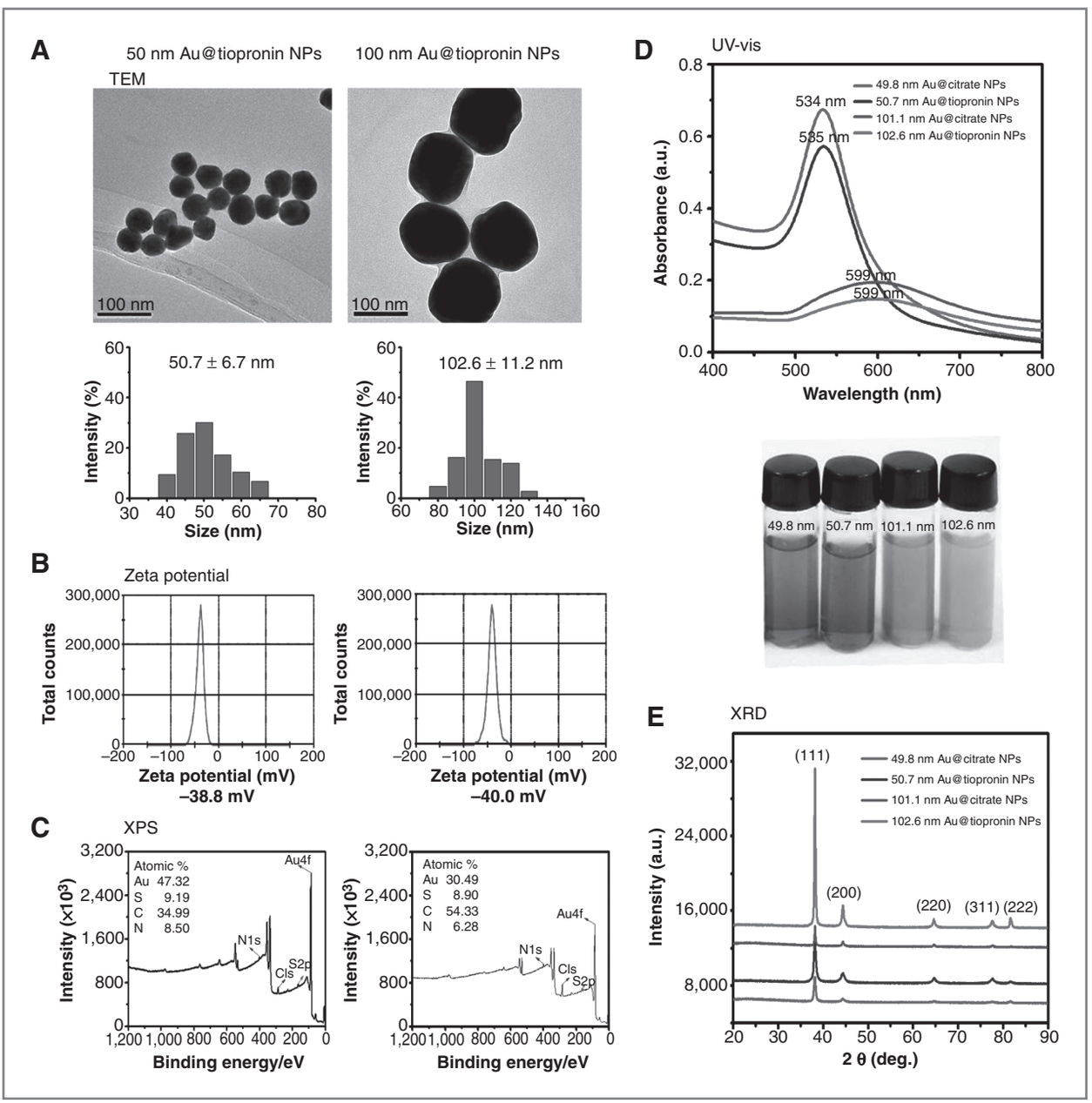

Figure 2. Characterization of 50 and 100 nm Au@tiopronin nanoparticles. A, TEM images and the corresponding size histograms of as-synthesized 50 and 100 nm gold nanoparticles coated with tiopronin. B, zeta potential of the 50 and 100 nm Au@tiopronin nanoparticles. C, XPS graph of the Au@tiopronin nanoparticles for 50 and 100 nm. D, visible spectrum of the Au@citrate and Au@tiopronin nanoparticles measuring 50 and 100 nm at wavelengths between 400 and 800 nm, and the corresponding photographs of nanoparticles dispersed in pure water. E, XRD patterns of as-synthesized Au@citrate and Au@tiopronin nanoparticles.

Published OnlineFirst October 16, 2012; DOI: 10.1158/0008-5472.CAN-12-2071

from −11.3 to −38.8 and −5.81 to −40.0 mV, respectively. The ζ-potential of gold nanoparticles mainly depends on the surface modification of the nanoparticles. For Au@citrate NPs, the potential was stabilized with citrate through the electrostatic interaction between gold nanoparticles and citrate. For Au@tiopronin NPs, the potential was stabilized with tiopronin through the formation of the Au–S bond. Free negatively charged carboxy groups of tiopronin were present and exposed on the outer surface of Au@tiopronin NPs. Therefore, the ζ-potential of Au@tiopronin NPs was lower than that of Au@citrate NPs.

XPS was used to investigate the different element components on the surface of gold nanoparticles. Figures 1C and 2C showed the atomic percentage of C, N, S, and Au on the surface of Au@citrate and Au@tiopronin NPs measuring 50 and 100 nm, which indicated that the molar ratio of S to Au of the 50 and 100 nm Au@citrate NPs were both 0.02; however, the ratio increased to 0.19 and 0.29 in the 50 and 100 nm Au@tiopronin NPs, respectively, showing that the thiol groups have been bonded to the surface of the gold nanoparticles. The similar molar ratio of N to Au was also observed at the same time.

Optical absorption spectra of the gold nanoparticles are related to the shape, size, and dispersion of the gold nanoparticles. When the size of Au@citrate NPs were 49.8 and 101 nm, their visible absorption peaks observed were situated at 534 and 599 nm, respectively (Fig. 2D). In general, with increasing size of gold nanoparticles, the corresponding surface plasmon resonance peaks would shift toward longer wavelength (29). Figure 2D shows that, after the surface exchange of tiopronin with corresponding Au@citrate NPs, the surface plasmon resonance peaks of the Au@tiopronin NPs essentially remained, which was consistent with the results shown in Figs. 1A and 2A. Meanwhile, the 50 and 100 nm gold nanoparticles that dispersed in pure water were purple red and yellow slurry in color. Thus, there was no significant difference in the visible spectrum between Au@citrate and the corresponding Au@tiopronin NPs.

On the other hand, the XRD patterns of all the gold nanoparticles could be indexed to the cubic form of gold with PDF number of 04-0784 (cubic, $a = b = c = 0.2884$ nm; $d\,(111) = 0.2355$ nm). As shown in Fig. 2E, there were 5 primary diffraction peaks at 38.187, 44.385, 64.576, 77.567, and 81.722, respectively, and these could be correspondingly indexed to the crystal planes of (111), (200), (220), (311), and (222) forms of Au. This result showed that the prepared material was definitely gold. Further observations showed that the peak shape was wider than that of the corresponding bulk material, which is one of the characteristics of nanocrystal materials, and while the particle is smaller, the corresponding XRD peak is wider (30). Moreover, calculations carried out on the basis of the (111) peak line-width at half-maximum intensity roughly showed that the average size of the nanoparticles were approximately 50 and 100 nm.

Taken together, the data discussed earlier show that we successfully prepared 50 and 100 nm Au@tiopronin NPs that are well dispersed in water and other relevant biologic media, including 0.9% saline, PBS, 5% glucose, and cell culture medium (Supplementary Fig. S2), are spherical in shape, and stable for more than 1 month at 4°C. More importantly, the only difference among these nanoparticles used in this study is the size, which was a requirement for the following studies.

Uptake of gold nanoparticles by monolayer cells

In this study, the concentration of gold nanoparticles was calculated from the concentration of gold by ICP-MS measurements for all the experiments according to the equation reported previously (19). First, the cell viability was investigated by the CCK-8 assay, and the data showed that the exposure to Au@tiopronin NPs for 24 hours was not toxic to the MCF-7 cells (Supplementary Fig. S3), suggesting that there was good biocompatibility of the nanoparticles; then, the MCF-7 cells were treated with 50 and 100 nm Au@tiopronin NPs at a concentration of 1 nmol/L. From the images taken under bright field microscopy in Fig. 3A, the uptake of 50 and 100 nm gold nanoparticles was observed. However, after the quantitative analysis by ICP-MS, the profile of the number of gold nanoparticles in each cell versus the size of gold nanoparticles indicated that the cellular uptake of gold nanoparticles occurred in a size-dependent manner at a concentration of 1 nmol/L nanoparticles with 24-hour treatment (Fig. 3B), that is, more uptake (more than 5 times) was observed for the 50 nm nanoparticle compared with that of the 100 nm nanoparticle. In addition, this result was in agreement with the reported maximum uptake by cells that occurred for the 50 nm citrate-stabilized gold nanoparticles (19). It has been reported that only monomeric "glycovirus" (∼50 nm) substantially entered cells via receptor-mediated endocytosis more efficiently than smaller or larger nanoparticles (31). Bio-TEM was carried out to obtain the intracellular distribution of the gold nanoparticles after treatment, and the images in Fig. 3C showed that both 50 and 100 nm gold nanoparticles were localized in the cytoplasm in an aggregated state after treatment for 24 hours, and the density of 50 nm gold nanoparticles observed in the cell was significantly more than that of the 100 nm gold nanoparticles, which is in accordance with the ICP-MS results.

Characterization of MCF-7 tumor spheroids

Multicellular tumor spheroids are 1 of the 3D culture systems that have been proven to have unique advantages over the 2D culture systems for cancer research (2, 12–14). Therefore, a spheroid of breast cancer cells (MCF-7) was developed as *ex vivo* tumor model in this study. To provide direct evidence of the morphology for the 3D culture, environmental scanning electron microscopy (ESEM) was carried out to show that MCF-7 cells formed tightly packed and rounded spheroids as shown in Fig. 4A. In the cellular spheroid, the cells are spindle shaped and the interactions between cells are very tight, which is similar to the state in *in vivo* tumor tissue while being different from the monolayer cells.

The cell condition in the spheroid was evaluated using qualitative hematoxylin and eosin (H&E) staining and quantitative flow cytometry. The results (Fig. 4B and C) indicated that cells in the spheroid model cultured for 7 days were able to be divided into 2 groups. One group comprised of metabolically active cells with larger size that could be stained with calcein AM by the live/dead cell vitality assay kit and were mainly

Published OnlineFirst October 16, 2012; DOI: 10.1158/0008-5472.CAN-12-2071

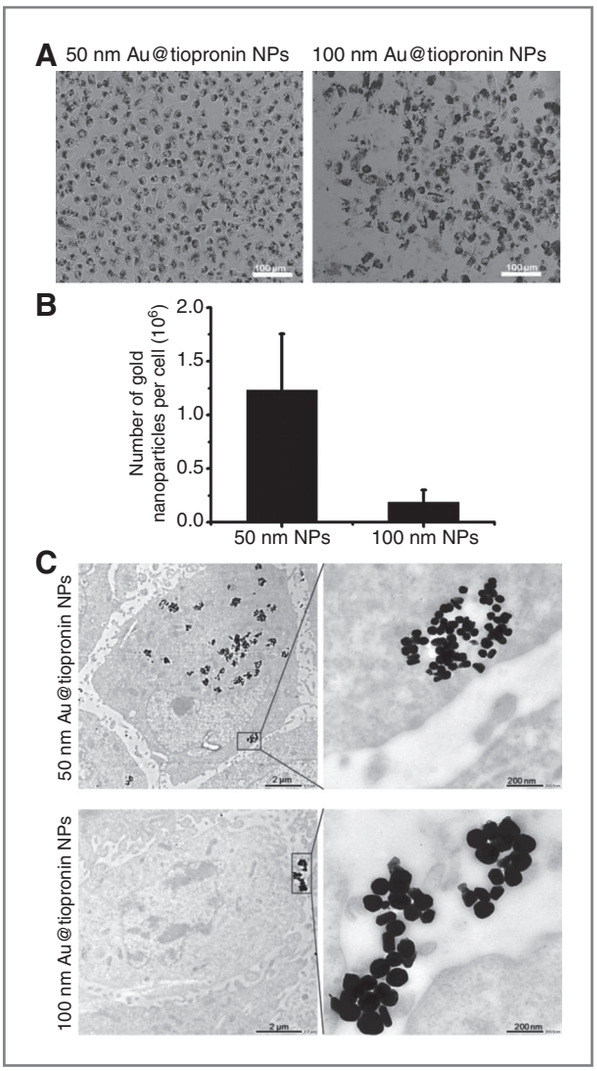

Figure 3. Cellular uptake of the 50 and 100 nm Au@tiopronin nanoparticles after incubation for 24 hours at a concentration of 1 nmol/L gold nanoparticles in the MCF-7 cells. A, images under bright field after treatment with the gold nanoparticles at a dose of 1 nmol/L nanoparticle. B, quantitative measurement of gold nanoparticles taken up by each cell by ICP-MS. C, representative TEM micrographs of the cellular uptake of the 50 nm and 100 nm Au@tiopronin nanoparticles.

localized in the outer part of the spheroids on H&E staining. Another group comprised of apoptotic or necrotic cells with smaller size, which could be stained with EthD-1 and were distributed in the inner parts of the spheroid. Furthermore, the cell conditions in the spheroid cultured for 14 days was similar to that in the spheroid cultured for 7 days, except that many more apoptotic and necrotic cells were observed with increasingthe culture time from 7 to 14 days.

These results show that the multicellular tumor spheroid used in this study was actually similar to the tumor tissue *in vivo*. Cells in the outer region of the spheroid were corresponding to the tumor tissue located beside the blood vessel, and the cells were proliferating with sufficient oxygen and nutrients. However, cells in the inner region were quiescent, similar to the tumor tissue located further away from the blood vessel, because of decreased availability of oxygen, nutrients, and pH (11, 13). Therefore, the tumor spheroid was a suitable model for evaluating the penetration behavior of gold nanoparticles.

Penetration behavior of gold nanoparticles into tumor spheroids

The penetration behavior of nanoparticles depends on their properties. For example, positive particles were taken up to a greater extent by proliferating cells, whereas negative particles were able to deliver drugs deep into tissues due to their ability to diffuse quickly (8). To enhance the nanoparticle delivery into the spheroid, arginine-glycine-aspartic acid peptide-conjugated dendrimers were developed, and they significantly enhanced the entry of dendrimer/siRNA nanoparticles into the U87 malignant glioma spheroid to improve siRNA delivery, which was presumably caused by the decreased integrin-binding affinity in the tumor model (32, 33). In this study, 50 and 100 nm Au@tiopronin NPs with the same surface properties were prepared, and this ensured the possibility of the size effect on the penetration behavior in the tumor spheroid.

Black spheroids were observed (Fig. 5A) after treatment with 50 and 100 nm gold nanoparticles at a concentration of 1 nmol/L for 3 and 24 hours, which is caused by the gold nanoparticles surrounding the spheroids compared with the spheroid without treatment. To confirm the exact location site of the gold nanoparticles in the spheroid, H&E staining and the corresponding dark-field microscopic observation were carried out. As shown in Fig. 5B, gold nanoparticles measuring 50 and 100 nm were primarily localized at the periphery of the spheroid at 3 hours after treatment, and the penetration of 50 nm nanoparticles increased with prolonging incubation time from 3 to 24 hours. However, 100 nm gold nanoparticles were hindered outside the tumor spheroid.

In addition, the quantitative analysis of ICP-MS data showed the number of gold nanoparticles in each spheroid (Fig. 5C). After 24-hour treatment, more penetration (more than 4 times) in the spheroids was observed at the nanoparticle size of 50 nm compared with that at the size of 100 nm. In addition, the concentration of gold nanoparticles in the tumor spheroid increased while prolonging the incubation time from 3 to 24 hours for the 50 nm gold nanoparticles, but not the 100 nm gold nanoparticles. This result is consistent with the report that the penetration of the nanoparticles into the spheroid core was limited to particles smaller than 100 nm (34). As mentioned above, the ECM presents a transport barrier that restricts nanoparticle penetration, and collagenase-coated 100 nm carboxylated polystyrene nanoparticles showed a 4-fold increase in the number of particles delivered to the spheroid core compared with the untreated nanoparticles due to the site-specific degradation of ECM proteins (34). Bio-TEM was used to evaluate the distribution of these nanoparticles in the spheroid in terms of microstructure, and Fig. 5D shows that the location site of 50 and 100 nm gold nanoparticles was only limited to the several layers of cells outside of the spheroid, and they were found only in the cytoplasm of each cell.

Published OnlineFirst October 16, 2012; DOI: 10.1158/0008-5472.CAN-12-2071

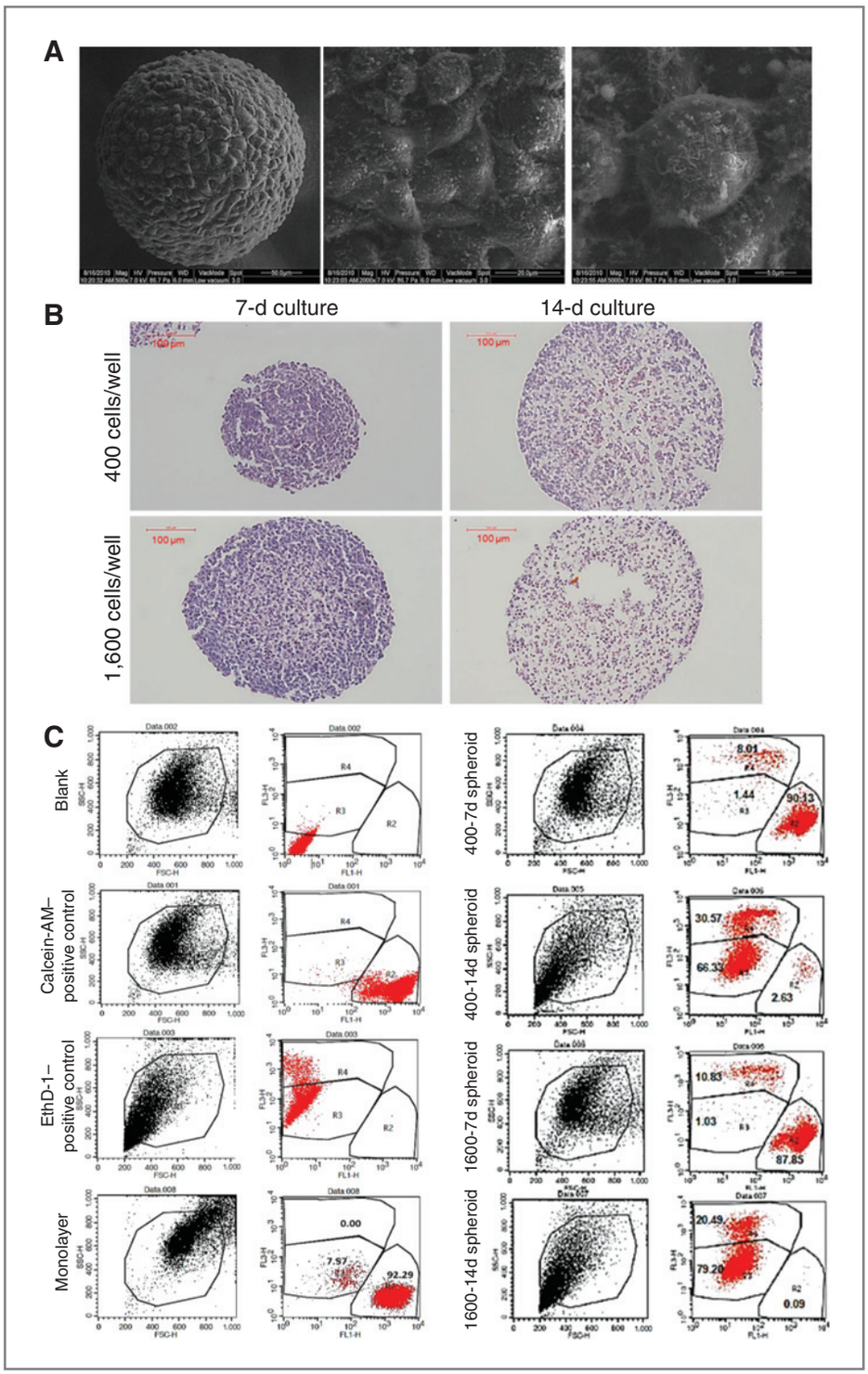

Figure 4. Characterization of MCF-7 multicellular tumor spheroid. A, morphology of both the monolayer cells and the 7-day-old spheroids at a seeding concentration of 600 cells per well observed by ESEM. B, images of the spheroids cultured for 7 days and 14 days at a seeding concentration of 400 or 1,600 cells per well after hematoxylin and eosin staining. C, cell conditions including live or dead cells in the spheroid with growth time of 7 days and 14 days at a seeding concentration of 800 cells per well analyzed by flow cytometry.

Pharmacokinetics and biodistribution of gold nanoparticles in tumor-bearing mice

Many types of nanoparticles used for drug delivery systems are approximately 100 nm in diameter due to the EPR effect of the leaky vasculature and poor lymphatic drainage associated with solid tumors (15, 35). The penetration of thenanoparticles from the blood into the tumor tissues primarily depends on diffusion and convection through endothelial fenestrae (36, 37). Moreover, high cell density, presence of the ECM, and interactions with cells also decreases the diffusion of

Published OnlineFirst October 16, 2012; DOI: 10.1158/0008-5472.CAN-12-2071

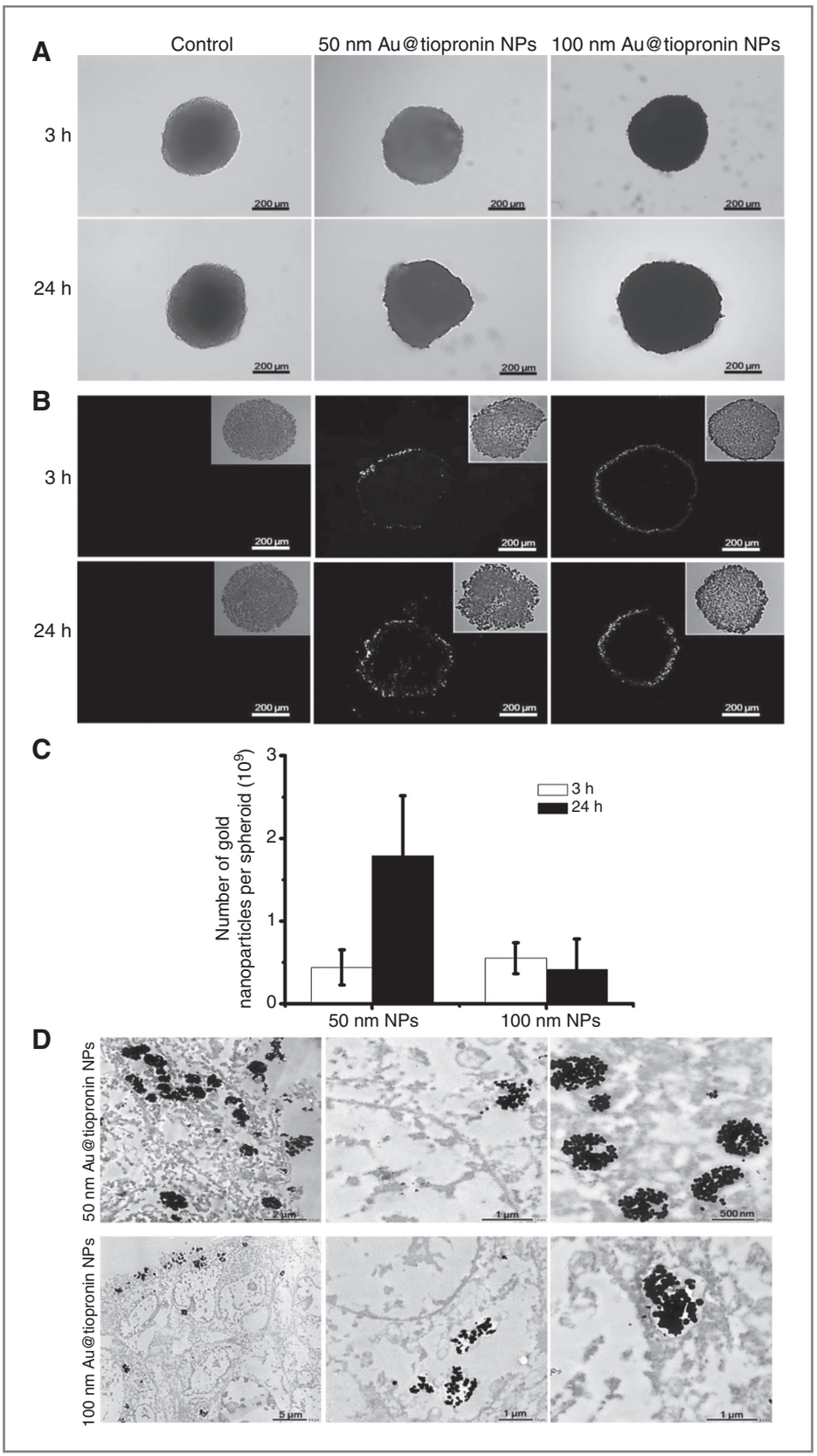

Figure 5. Penetration behavior of the 50 and 100 nm Au@tiopronin nanoparticles into the MCF-7 tumor spheroid at a concentration of 1 nmol/L for 3 and 24 hours. A, images under bright field after treatment with the gold nanoparticles. B, images after H&E staining and under dark field after culture with the nanoparticles. C, ICP-MS analysis of the number of Au@tiopronin nanoparticles in each treated spheroid. D, representative TEM images including the external and internal region of the treated spheroid for 24 hours.

Published OnlineFirst October 16, 2012; DOI: 10.1158/0008-5472.CAN-12-2071

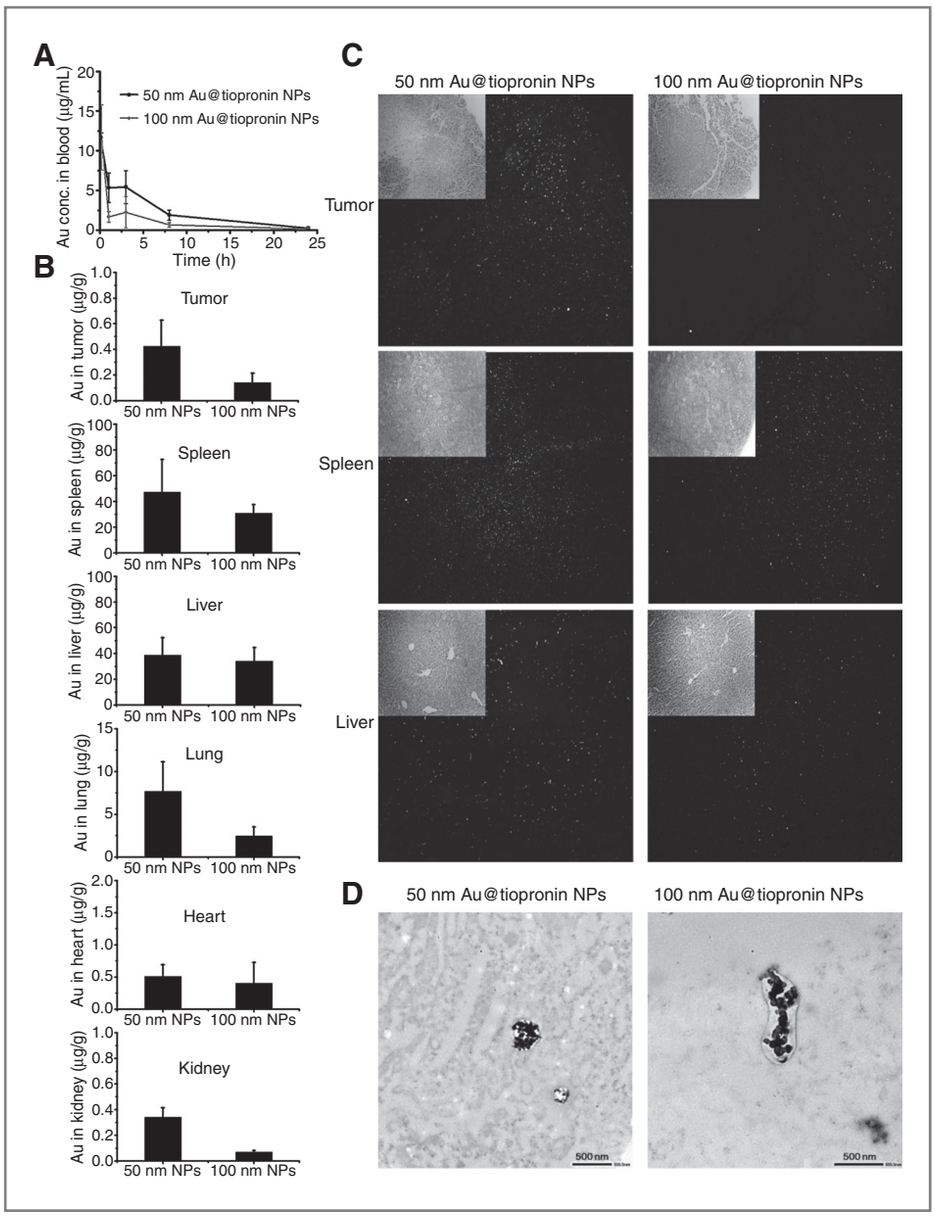

Figure 6. Blood elimination profiles and biodistribution of the 50 and 100 nm Au@tiopronin nanoparticles at a dose of 5 mg Au/kg after intravenous administration. A, blood elimination profiles of gold following a single intravenous injection of 50 and 100 nm Au@tiopronin nanoparticles at a dose of 5 mg Au/kg in the tumor-bearing mice. Data represent mean ± SD ($n = 3$). B, gold content in the tissues including tumor, heart, liver, spleen, lung, and kidney at 24 hours after intravenous injections of gold nanoparticles. Data represent mean ± SD ($n = 3$). C, images of tumor, liver, and spleen after H&E staining and the corresponding images observed under dark field. D, Bio-TEM images of the tumor tissue taken 24 hours after the administration of the Au@tiopronin nanoparticles.

nanoparticles into the tumor compartment. To improve the accumulation of the nanoparticles in the tumor, active targeting can be used to increase cellular internalization and reduce the clearance of nanoparticles from the tumor interstitium (38).

To evaluate the accumulation behavior of 50 and 100 nm gold nanoparticles in the tumor tissue *in vivo*, the tumor-bearing mice were developed. At first, the pharmacokinetic behavior of the nanoparticles was investigated after a single 5 mg Au/kg intravenous injection, and the data indicated that all of the nanoparticles were eliminated rapidly from the blood (Fig. 6A). The concentration of Au in blood decreased to 11.0 μg/mL at 10 minutes and 1.9 and 0.2 μg/mL at 8 and 24 hours for 50 nm nanoparticles, respectively. To some extent, the 100 nm nanoparticles were cleared faster from the blood than the 50 nm nanoparticles. The pharmacokinetics of the nanoparticles can be influenced by many factors mainly including the size and surface properties of the nanoparticles affect the extent of opsonization and clearance. In addition, the presence of a nonionic, steric stabilizing hydrophilic polymer such as polyethelene glycol (PEG) has been shown to prolong the circulation time of the nanoparticles by avoiding opsonization and subsequent clearance by the mononuclear phagocytic system (38). Gold nanoparticles used in this study were coated with tiopronin, and they were opsonized easily by the proteins and then cleared from the blood.

With regard to the accumulation of gold nanoparticles in tumor, more amount of gold was detected after 24 hours of

Published OnlineFirst October 16, 2012; DOI: 10.1158/0008-5472.CAN-12-2071

administration for 50 nm NPs (0.42 μg/g) and less for 100 nm NPs (0.14 μg/g; Fig. 6B). In other tissues, 50 and 100 nm gold nanoparticles accumulated dominantly in the liver and spleen, constituting a total percentage of more than 80% of the injected dose. Furthermore, only small amounts of nanoparticles were distributed in the tissues of lung and heart (Supplementary Table S1). Following the quantitative analysis of gold content in the tissue, H&E staining and corresponding dark-field microscopic analysis were also conducted to observe the site where gold nanoparticles were distributed. As shown in Fig. 6C and D, the 50 nm gold nanoparticles showed a little more amount than 100 nm gold nanoparticles in the tumor tissue (Fig. 6C and D), and a nonhomogeneous distribution of gold nanoparticles was observed. It is speculated that the nanoparticles were mainly distributed beside the blood vessels, especially for the larger 100 nm gold nanoparticles. In the liver and spleen, the distribution of gold nanoparticles is more obvious. However, no obvious gold nanoparticles were observed in other tissues such as the kidneys, lungs, and heart (Supplementary Fig. S4).

Recently, researchers have gradually realized that the penetration of the nanoparticles into a tumor is definitely important for the drug delivery system and it should not be neglected. To improve the nanoparticle delivery into tumors, functional nanoparticles, where the size of the nanoparticles shrank from 100 to 10 nm triggered by the matrix metalloproteinases overexpressed in the tumor microenviroment, exhibited both long circulation half-life necessary for the EPR effect and the deep tumor penetration for delivery into the tumor tissues *in vivo* (17). In addition, a novel approach of the noncovalent drug delivery by PEGylated Au NPs showed surprisingly efficient drug release and deep penetration into the center of tumor tissues (39). Taken together, the size of the nanomedicines critically affects the penetration and efficacy of the drugs in tumors.

Conclusion

In summary, our study provides new insights into the size effect of gold nanoparticles measuring 50 and 100 nm on the localization and penetration behavior using 2D culture *in vitro*, 3D culture of multicellular tumor spheroid *ex vivo*, and xenograft tumor model *in vivo*. Although the tumor microenvironment significantly limited the deep penetration of nanoparticles into tumor tissue, the smaller gold nanoparticles (50 nm) showed more advantages over the larger nanoparticles (100 nm) in the uptake and permeability in tumor tissues. Researchers have placed great importance on the prolonged circulation and altered biodistribution of the nanoparticle-based drug delivery systems; however, the tumor uptake and tissue penetration of the nanoparticles is another key issue for exerting effective cancer therapy. More importantly, this study reveals that smaller nanoparticles are more effective than larger particles at delivering drugs to tumor cells, with implications for many types of cancer nanotherapeutic studies.

Disclosure of Potential Conflicts of Interest

No potential conflicts of interest were disclosed.

Authors' Contributions

Conception and design: S. Huo, H. Ma, S. He, X-J. Liang
Development of methodology: S. Huo, K. Huang, S. He, X-J. Liang
Acquisition of data (provided animals, acquired and managed patients, provided facilities, etc.): S. Huo, H. Ma, K. Huang, T. Wei, S. He, X-J. Liang
Analysis and interpretation of data (e.g., statistical analysis, biostatistics, computational analysis): S. Huo, H. Ma, K. Huang, S. Jin, S. He, X-J. Liang
Writing, review, and/or revision of the manuscript: S. Huo, H. Ma, K. Huang, S. Jin, S. He, X-J. Liang
Administrative, technical, or material support (i.e., reporting or organizing data, constructing databases): S. Huo, H. Ma, K. Huang, S. Jin, J. Zhang, S. He, X-J. Liang
Study supervision: S. Huo, J. Liu, S. He, X-J. Liang

Grant Support

This work was financially supported by the Chinese Natural Science Foundation project (grant nos. 30970784, 81171455, and 31100720), National Key Basic Research Program of China (grant no. 2009CB930200), Chinese Academy of Sciences (CAS) "Hundred Talents Program" (grant no. 07165111ZX), CAS Knowledge Innovation Program and Tianjin Research Program of Applied Basic & Cutting-edge Technologies (grant no. 09JCYBJC27200). The authors are also thankful for the support from the joint lab of nanotechnology for bioapplication, which was established with Life Technologies Corp. in the National Center for Nanoscience and Technology of China.

The costs of publication of this article were defrayed in part by the payment of page charges. This article must therefore be hereby marked *advertisement* in accordance with 18 U.S.C. Section 1734 solely to indicate this fact.

Received May 25, 2012; revised October 3, 2012; accepted October 8, 2012; published OnlineFirst October 16, 2012.

References

1. Campbell RB, Fukumura D, Brown EB, Mazzola LM, Izumi Y, Jain RK, et al. Cationic charge determines the distribution of liposomes between the vascular and extravascular compartments of tumors. Cancer Res 2002;62:6831–6.
2. Minchinton AI, Tannock IF. Drug penetration in solid tumours. Nat Rev Cancer 2006;6:583–92.
3. Brown JM, Giaccia AJ. The unique physiology of solid tumors: opportunities (and problems) for cancer therapy. Cancer Res 1998;58:1408–16.
4. Brown JM, Wilson WR. Exploiting tumour hypoxia in cancer treatment. Nat Rev Cancer 2004;4:437–47.
5. Padera TP, Stoll BR, Tooredman JB, Capen D, di Tomaso E, Jain RK. Pathology: cancer cells compress intratumour vessels. Nature 2004; 427:695.
6. Cabral H, Matsumoto Y, Mizuno K, Chen Q, Murakami M, Kimura M, et al. Accumulation of sub-100 nm polymeric micelles in poorly permeable tumours depends on size. Nat Nanotechnol 2011;6: 815–23.
7. Chauhan VP, Popovic Z, Chen O, Cui J, Fukumura D, Bawendi MG, et al. Fluorescent nanorods and nanospheres for real-time *in vivo* probing of nanoparticle shape-dependent tumor penetration. Angew Chem Int Ed Engl 2011;50:11417–20.
8. Kim B, Han G, Toley BJ, Kim CK, Rotello VM, Forbes NS. Tuning payload delivery in tumour cylindroids using gold nanoparticles. Nat Nanotechnol 2010;5:465–72.
9. Kim JA, Aberg C, Salvati A, Dawson KA. Role of cell cycle on the cellular uptake and dilution of nanoparticles in a cell population. Nat Nanotechnol 2012;7:62–8.
10. Perrault SD, Walkey C, Jennings T, Fischer HC, Chan WC. Mediating tumor targeting efficiency of nanoparticles through design. Nano Lett 2009;9:1909–15.

Published OnlineFirst October 16, 2012; DOI: 10.1158/0008-5472.CAN-12-2071

11. Fracasso G, Colombatti M. Effect of therapeutic macromolecules in spheroids. Crit Rev Oncol Hematol 2000;36:159–78.
12. Lin RZ, Chang HY. Recent advances in three-dimensional multicellular spheroid culture for biomedical research. Biotechnol J 2008;3:1172–84.
13. Ong SM, Zhao Z, Arooz T, Zhao D, Zhang S, Du T, et al. Engineering a scaffold-free 3D tumor model for *in vitro* drug penetration studies. Biomaterials 2010;31:1180–90.
14. Pickl M, Ries CH. Comparison of 3D and 2D tumor models reveals enhanced HER2 activation in 3D associated with an increased response to trastuzumab. Oncogene 2009;28:461–8.
15. Maeda H, Wu J, Sawa T, Matsumura Y, Hori K. Tumor vascular permeability and the EPR effect in macromolecular therapeutics: a review. J Control Release 2000;65:271–84.
16. Tong R, Hemmati HD, Langer R, Kohane DS. Photoswitchable nanoparticles for triggered tissue penetration and drug delivery. J Am Chem Soc 2012;134:8848–55.
17. Wong C, Stylianopoulos T, Cui J, Martin J, Chauhan VP, Jiang W, et al. Multistage nanoparticle delivery system for deep penetration into tumor tissue. Proc Natl Acad Sci U S A 2011;108:2426–31.
18. Chithrani BD, Chan WC. Elucidating the mechanism of cellular uptake and removal of protein-coated gold nanoparticles of different sizes and shapes. Nano Lett 2007;7:1542–50.
19. Chithrani BD, Ghazani AA, Chan WC. Determining the size and shape dependence of gold nanoparticle uptake into mammalian cells. Nano Lett 2006;6:662–8.
20. Jiang W, Kim BYS, Rutka JT, Chan WCW. Nanoparticle-mediated cellular response is size-dependent. Nat Nanotechnol 2008;3:145–50.
21. Lu F, Wu SH, Hung Y, Mou CY. Size effect on cell uptake in well-suspended, uniform mesoporous silica nanoparticles. Small 2009;5:1408–13.
22. Lundqvist M, Stigler J, Elia G, Lynch I, Cedervall T, Dawson KA. Nanoparticle size and surface properties determine the protein corona with possible implications for biological impacts. Proc Natl Acad Sci U S A 2008;105:14265–70.
23. Goldsborough AS, Handley MD, Dulcey AE, Pluchino KM, Kannan P, Brimacombe KR, et al. Collateral sensitivity of multidrug resistant cells to the orphan drug tiopronin. J Med Chem 2011;54:4987–97.
24. Dahl JA, Maddux BLS, Hutchison JE. Toward greener nanosynthesis. Chem Rev 2007;107:2228–69.
25. Kumar A, Ma HL, Zhang X, Huang KY, Jin SB, Liu J, et al. Gold nanoparticles functionalized with therapeutic and targeted peptides for cancer treatment. Biomaterials 2012;33:1180–9.
26. Frens G. Controlled nucleation for regulation of particle-size in monodisperse gold suspensions. Nature-Physical Sci 1973;241:20–2.
27. Jana NR, Gearheart L, Murphy CJ. Evidence for seed-mediated nucleation in the chemical reduction of gold salts to gold nanoparticles. Chem Mater 2001;13:2313–22.
28. Friedrich J, Seidel C, Ebner R, Kunz-Schughart LA. Spheroid-based drug screen: considerations and practical approach. Nat Protocols 2009;4:309–24.
29. Haiss W, Thanh NT, Aveyard J, Fernig DG. Determination of size and concentration of gold nanoparticles from UV-vis spectra. Anal Chem 2007;79:4215–21.
30. Petkov V, Peng Y, Williams G, Huang BH, Tomalia D, Ren Y. Structure of gold nanoparticles suspended in water studied by x-ray diffraction and computer simulations. Phys Rev B 2005;72:195402.
31. Osaki F, Kanamori T, Sando S, Sera T, Aoyama Y. A quantum dot conjugated sugar ball and its cellular uptake. On the size effects of endocytosis in the subviral region. J Am Chem Soc 2004;126:6520–1.
32. Waite CL, Roth CM. PAMAM-RGD conjugates enhance siRNA delivery through a multicellular spheroid model of malignant glioma. Bioconjug Chem 2009;20:1908–16.
33. Waite CL, Roth CM. Binding and transport of PAMAM-RGD in a tumor spheroid model: the effect of RGD targeting ligand density. Biotechnol Bioeng 2011;108:2999–3008.
34. Goodman TT, Olive PL, Pun SH. Increased nanoparticle penetration in collagenase-treated multicellular spheroids. Int J Nanomedicine 2007;2:265–74.
35. Matsumura Y, Maeda H. A new concept for macromolecular therapeutics in cancer chemotherapy: mechanism of tumoritropic accumulation of proteins and the antitumor agent smancs. Cancer Res 1986;46:6387–92.
36. Jain RK. Molecular regulation of vessel maturation. Nat Med 2003;9:685–93.
37. Jang SH, Wientjes MG, Lu D, Au JL. Drug delivery and transport to solid tumors. Pharm Res 2003;20:1337–50.
38. Mikhail AS, Allen C. Block copolymer micelles for delivery of cancer therapy: transport at the whole body, tissue and cellular levels. J Control Release 2009;138:214–23.
39. Cheng Y, Meyers JD, Broome AM, Kenney ME, Basilion JP, Burda C. Deep penetration of a PDT drug into tumors by noncovalent drug-gold nanoparticle conjugates. J Am Chem Soc 2011;133:2583–91.

Cancer Research
The Journal of Cancer Research (1916–1930) | The American Journal of Cancer (1931–1940)

AACR American Association for Cancer Research

Superior Penetration and Retention Behavior of 50 nm Gold Nanoparticles in Tumors

Shuaidong Huo, Huili Ma, Keyang Huang, et al.

Cancer Res 2013;73:319-330. Published OnlineFirst October 16, 2012.